CFD Letters www.cfdl.issres.net Vol. 2 (3) – September 2010

Axisymmetric Vortex Simulations with Various Turbulence Models

Brian H. Fiedler[1c] and Gabriel S. Garfield[2]

[1] *School of Meteorolgy, University of Oklahoma, U.S.A*
[2] *Cooperative Institute for Mesoscale Meteorological Studies, University of Oklahoma, U.S.A*

Received: 07/08/2010 – Revised 28/09/2010 – Accepted 15/10/2010

Abstract

The CFD code **FLUENT**™ has been applied to a vortex within an updraft above a frictional lower boundary. The sensitivity of vortex intensity and structure to the choice of turbulent model is explored. A high Reynolds number of 10^8 is employed to make the investigation relevant to the atmospheric vortex known as a *tornado*. The simulations are axisymmetric and are integrated forward in time to equilibrium. In a variety of turbulence models tested, the Reynolds Stress Model allows for the greatest intensification of the vortex, with the azimuthal wind speed near the surface being 2.4 times the speed of the updraft, consistent with the destructive nature of tornadoes. The Standard $k-\varepsilon$ Model, which is simpler than the Reynolds Stress Model but still more detailed than what is commonly available in numerical weather prediction models, produces an azimuthal wind speed near the surface of at most 0.6 times the updraft speed.

Keywords: tornado; turbulence modelling; k-epsilon models; vortex flow; reynolds-stress models

1. Introduction

1.1 Tornadoes

As a subject of science, a tornado presents a number of scientific questions. Within the realm of fundamental fluid dynamics, one question is: What limits the maximum wind speed? In pursuit of an answer, we can rephrase the question: For a vortex embedded in an updraft, what processes limit the stretching and intensification of the vortex? Phrased that way, the pursuit leads us to experiments with desktop devices and computers, with configurations much simpler than either the atmospheric manifestation of tornadoes or the state-of-art simulations of tornadic storms [1].

Desktop investigations must reckon with the fact that the Reynolds number of a thunderstorm is of order $Re = 10^{10}$, based on an updraft speed of 50 ms⁻¹ [1], a depth of the troposphere of 10^4 m and a kinematic viscosity of air of order 2×10^{-5} m^{2}s^{-1}. Laboratory and numerical simulations will need to make compromises in employing such a large Reynolds

[c] Corresponding author: B. H. Fiedler
Email: bfiedler@ou.edu

number. One possible compromise for a numerical simulations is to model only the effect of turbulent mixing on a predicted ensemble-mean flow, using a so-called "turbulence parameterization". Another compromise is to constrain the solution to be axisymmetric, which further reduces the need for computer resources. Both of these compromises are made here, which allows the numerical simulations to proceed with modest resources on a desktop computer.

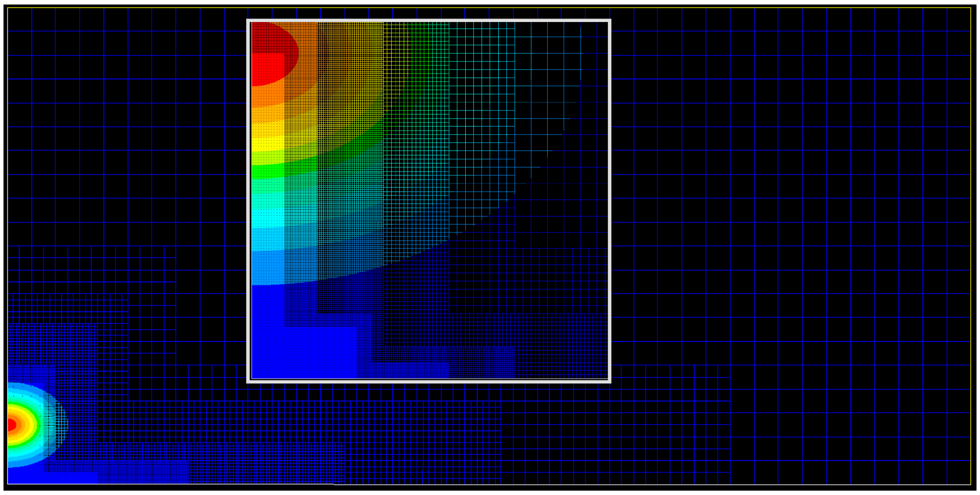

Figure 1. The entire domain, with contours of the body force b at the lower left. The inset figure shows only 0<r<0.58 and 0<z<0.58, and is able to display the finest three grid nests.

Requiring solutions to be axisymmetric is not absolutely essential on today's computers, but it certainly expedites a rapid exploration of the vortex solutions. However, it is known from Fiedler [2] that for $Re \geq 2.5 \times 10^3$, fully three-dimensional simulations have transient events and spiral vortex breakdowns, events that are not possible in axisymmetric simulations. Nevertheless, Fiedler [2] shows the intensity of axisymmetric simulations differ from the three-dimensional simulations in a systematic way. Knowledge of those systematic differences enhances the value of the axisymmetric simulations presented here. Axisymmetric simulations are a reasonable first step in exploring the sensitivity of tornado simulations to the turbulence model.

1.2 Turbulence Models

The numerical model we employ is the commercial CFD code **FLUENT™** version 6.3. **FLUENT™** uses the finite-volume method to discretize the equations of fluid flow. Four turbulence models are available in **FLUENT™** . Within the four models, various options and adjustments are possible. Given the popularity of **FLUENT™** , there are many publications that review the governing equations of these turbulence models[1] and that summarize the differences. Only a summary of the models will be presented here.

The first three models predict an eddy-viscosity μt, which is related to turbulent kinetic energy k and the rate of dissipation of turbulent kinetic energy ε by:

$$\mu_t = \rho C_\mu \frac{k^2}{\varepsilon} \, , \qquad (1)$$

1 http://www.cfd-online.com/Wiki/category:Turbulence_models

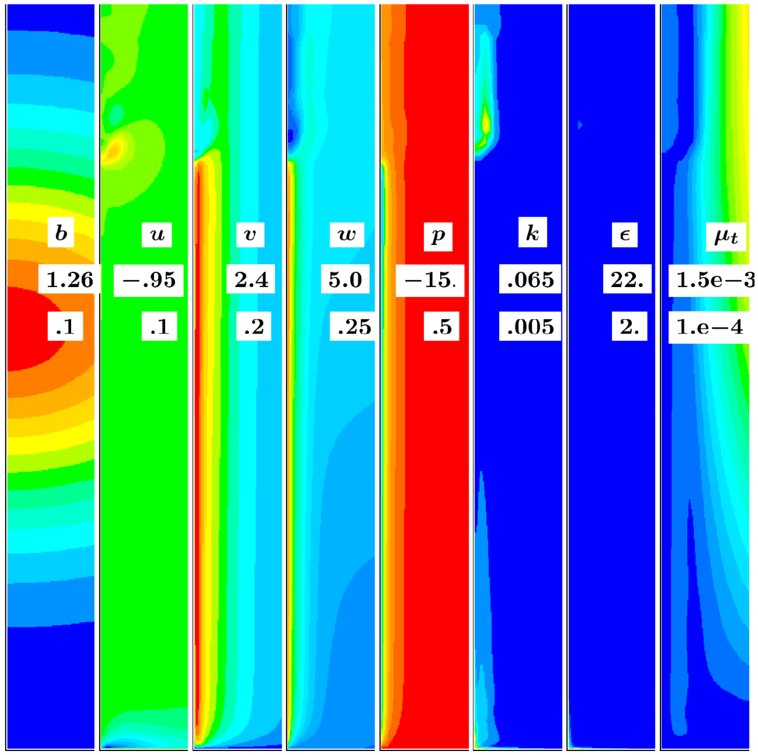

Figure 2. The steady solution with f =.003, Re=10^8, and RSM. Note the vortex break down event aloft. The upper number is the maximum in the plot, the lower number is the contour interval, all dimensionless. b is body force, u radial velocity, v azimuthal velocity, w axial velocity, k turbulent kinetic energy, ε dissipation rate of turbulent kinetic energy, μ_t turbulent viscosity.

where ρ is the mass density and C_μ is a constant. Of these three models, two of the models, the $k-\varepsilon$ model and the RNG $k-\varepsilon$ model (hereafter RNG model) employ a convection-diffusion equation for k and ε, with production and dissipation terms. The third model, the $k-\omega$ model, emphasizes a convection-diffusion equation for the specific dissipation rate ω:

$$\omega \equiv \frac{\varepsilon}{k} \tag{2}$$

Rather than for ε. The RNG model differs from the k-ε model in that the production and dissipation terms in the prognostic equations for k and ε employ different coefficients and, more importantly, the prognostic equation for ε employs a new production/dissipation term, R_ε. As compared with the standard term for dissipation of ε, the new term can change sign at high rates of strain and become a production term for ε, which reduces k and thus reduces μ_t by decreasing the numerator and increasing the denominator of (1).

The User's Guide for **FLUENT™** promotes the use of RNG for swirling flows; with the claim "the RNG model is more responsive to the effects of rapid strain and streamline curvature than the standard $k-\varepsilon$ model, which explains the superior performance of the RNG model for certain classes of flows". Similarly, the $k-\omega$ model is cited for abilities with "plane, round and radial jets". Consistent with these recommendations, Bartosiewicz et al. [3] cite $k-\omega$ as superior to RNG in simulations of supersonic ejectors, and Gupta and Kumar [4] find RNG superior to $k-\varepsilon$ in simulations of swirling flow in a cylinder. Indeed, **FLUENT™** prominently features a default RNG option for "Swirl Dominated Flow" and an adjustable swirl factor, making RNG an attractive choice for attempts to simulate a confined vortex. Nevertheless, Saqr *et al.* [5] review the criticisms of the tortuous theoretical derivation of the RNG coefficients, and present a modified version of RNG, which is simply the standard $k-\varepsilon$ model, but with the R_ε term from the RNG model included in it. They find their modified model, applied to a confined vortex, provided better agreement with their laboratory measurements, than did the formal RNG model.

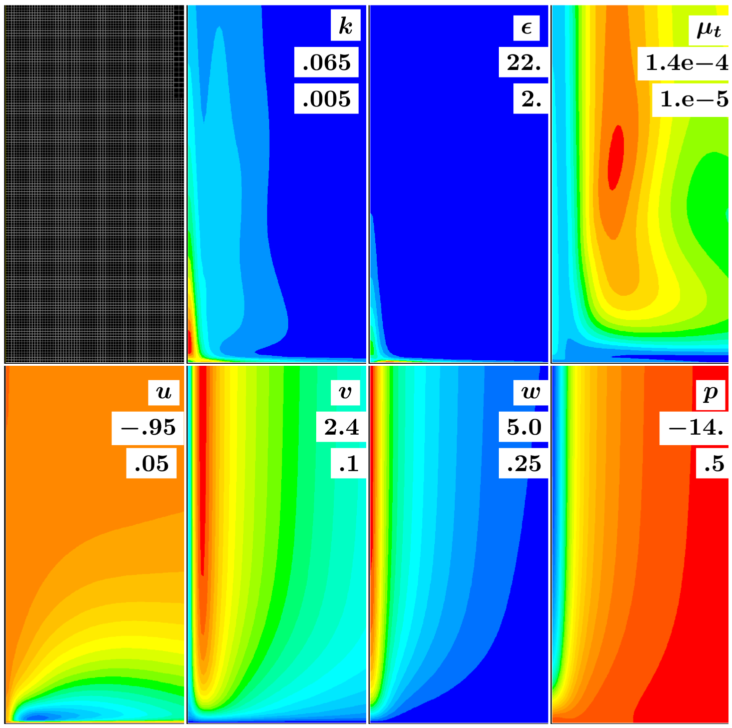

Figure 3. As in figure 2, but only to z=.105 and r=.055. The radial convergence produces an axial jet in the core of the vortex. A local minimum in μ_t, occurs where v is a minimum.

The fourth turbulence model under consideration is the Reynolds Stress Model (RSM). Unlike the first three models, the RSM does not employ an isotropic eddy viscosity. The Reynolds stresses are forecasted with convection-diffusion equations, and with these equations requiring closure assumptions. The **FLUENT™** User's Guide states that "the RSM accounts for the effects of streamline curvature, swirl, rotation and rapid changes in strain rate in a more rigorous manner than one-equation and two-equation models". In comparisons of simulations of a gas cyclone separator with experimental data, Xiang and Lee [6] find the RSM superior to the other options, as does Hoekstra et al. [7].

2. Model Configuration

The model domain is cylindrical, as in Fiedler [8] and in the axisymmetric experiments of Fiedler [9] and Fiedler [2], but extended to four times the size (Figure 1). A fixed body force *b* on the axis provides acceleration of an updraft. The cylindrical domain is set to be rotating about the axis; a Coriolis force provides the generation of relative axial vorticity. The magnitude of Coriolis force, per unit mass, is 2Ω times the magnitude of the horizontal velocity vector, where Ω is the rotation rate of the domain about the axis, which is easily set within **FLUENT™**. 2Ω will be referred to as *f*, the Coriolis parameter.

FLUENT™ uses physical quantities defined with S.I. units. However, with the proper choice of model parameters, dimensionless values for a more universal dimensionless model are merely the dimensional quanties with the S.I. units removed. At the end of this section, and after, only the dimensionless values will be cited.

The model domain extends with axial dimension 0 m ≤ z ≤ 4 m and radial dimension 0 m ≤ r ≤ 8 m. Acting alone, the body force would accelerate a parcel, initially at rest, up to a speed of 1 m s^{-1}. The fluid is incompressible, with density set to 1 kg m^{-3}. For calculating a Reynolds number, the length scale is the lower 1 m, which is the length that surrounds the significant body force and the height of original domain used in Fiedler [8]. That original, smaller domain had an imposed damping region in the upper half. In this larger domain, no imposed damping is required. (The nesting capabilities of **FLUENT™** allow the use of a larger domain with trivial additional expense in computer resources). At the lower boundary, the roughness length is .001 m, and used with the default option of Standard Wall Functions. The other boundaries are free-slip (symmetry). In most simulations, the dynamic viscosity is set to 10^{-8} kg m^{-1} s^{-1}, thus the Reynolds number is $Re=10^8$.

The **FLUENT™** solver was pressure based, Green-Gauss cell based, using axisymmetric swirl space, the relative velocity formulation, with 2nd-order implicit time-stepping. The grid elements are square. The largest grid size is 0.2, the smallest grid size is 0.2×2^{-7} = .00156. For a speed of 1 (actual speeds in the simulations can exceed 5), the time to cross the smallest grid size is .00156. The solutions shown here used a time step of 0.001 with 10 iterations per time step. Unless stated otherwise, the advection scheme was 3rd-order MUSCL for momentum and first-order upwind for k and ε 3rd-order offering no significant improvement for k and ε . The other solution controls, for example the under-relaxation factors, remained at the defaults for **FLUENT™** . Except for some oscillatory solutions when using the RNG turbulence scheme, the solutions asymptotically approach a steady state. If the Coriolis parameter f is not altered, a turbulence model can be changed and a new steady state is achieved within 30 time units or less.

Numerous experiments were done with various model configurations. Neither a larger domain, an additional nested grid, nor a smaller time step, nor additional iterations per time step has a significant impact on the final equilibrium solution.

3. The Results

Figure 2 shows contours of one the most intense solutions. Most of the vortex is columnar, with little variation along the axial direction. The pressure p shown here is the pressure deviation from that at the mid-height of the outer wall, r=8 and $z=2$ (in other words, those coordinates are the zero point for the plotted pressure). A hydrostatic pressure deficit beneath b would reach a minimum of $p=-0.5$ at z = 0 and r = 0. In the simulation, the pressure minimum of p = −15 is 30 times the hydrostatic value. There is an axial jet inside the core of the vortex with speed maximum w=5. Recall that b acting alone would generate an updraft with w=1. The axial jet is essential for levitating the vortex breakdown, thus preventing a downdraft from filling in the vortex from above and relieving the low pressure [10,8]. Convergence induced by friction in the boundary layer is essential for producing the axial jet.

The lower part of the vortex of figure 2 is shown in figure 3, where the radial convergence leading to an axial jet is clearly evident. The RSM does not have an isotropic diffusivity for momentum. A turbulent diffusivity μ_t is plotted, but it is the one for turbulent diffusion for scalars. This diffusivity will allow for a comparison with the other three models, which do have an isotropic diffusivity for momentum. Note the large values of ε and k in the corner region, but large values of μ_t are outside the vortex and the boundary layer. In fact, at the radius of maximum v, μ_t is a minimum.

As in Fiedler [2] and Lewellen and Lewellen [11], we use the subscripted symbol I to denote the intensity of the subscripted quantity, meaning the ratio of the maximum of the quantity to a reference value. For velocity components, the reference value is 1, so I_w , I_v , and I_u will simply be the maximum value in the vortex. But since we are interested in the radial inflow into the tornado, I_u will be the maximum of $-u$. For the purpose of plotting pressure intensity with a scale similar to that for velocity, we define $q \equiv \sqrt{-2\,p}$. Figure 4 shows I_q, I_w, I_v and I_u in the nearly-steady asymptotic solutions, spanning a decade of values of f. The corresponding contour plot for v in these 21 solutions is shown in Figure 5. For some values of f, solutions are not presented for $k\!-\!\varepsilon$ and $k\!-\!\omega$ because no concentrated vortex was identifiable. The progression of vortex structure, with increasing inputs of "swirl" (which here is controlled with f), from a weak slender vortex with a central updraft to wide vortex with a central downdraft, is a well-known feature of laminar solutions of a vortex in an updraft above a lower boundary with friction [8,2], and in turbulent solutions [12].

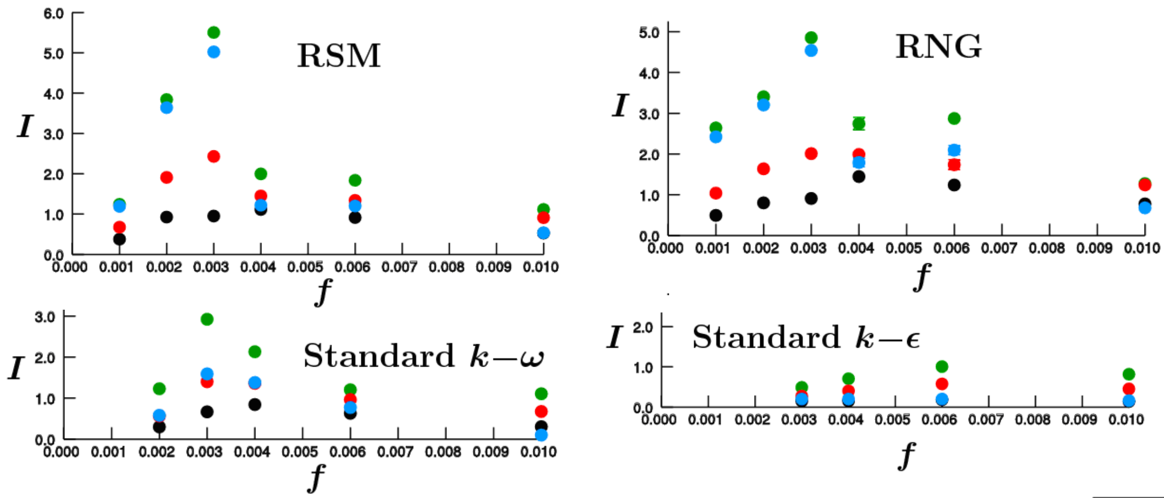

Figure 4. Intensity of q, w, v and u as a function of f for four turbulence models with Re=10^8. $q \equiv \sqrt{-2p}$. The slight variance in some oscillatory RNG solutions is indicated by error bars.

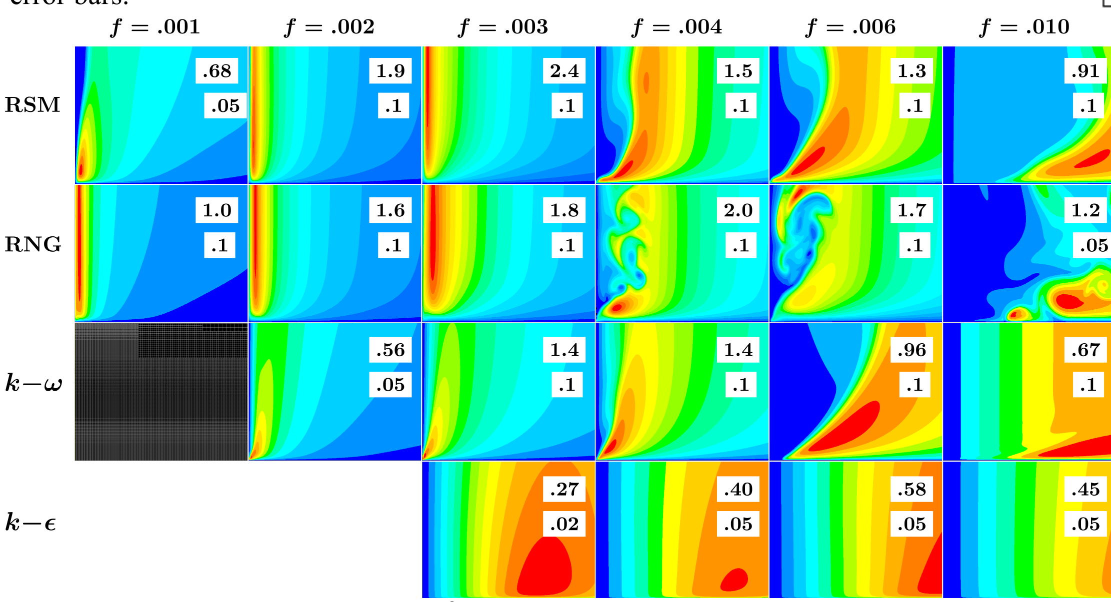

Fig. 5: v as a function of f at Re = 10^8 for the solutions in figure 4. Region shown is to z=0.105 and r = 0.14.

Figure 6 and Figure 7 show that the solutions using RNG become independent of Re for $Re > 10^7$; this independence at large Re is known as *Reynolds-number similarity* [13]. Presumably, the behavior with the other turbulence models also display Reynolds-number similarity.

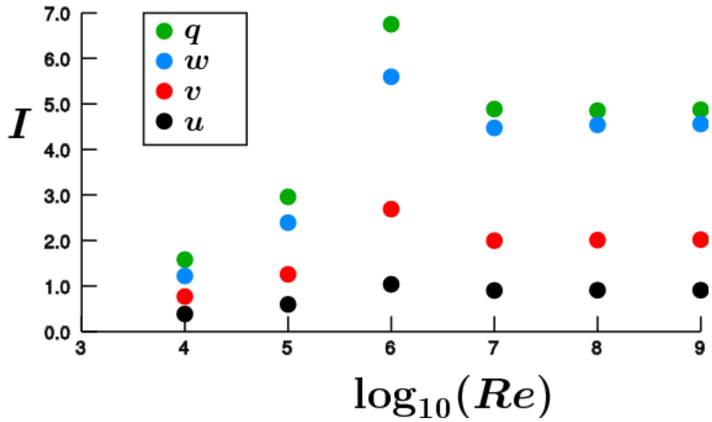

Figure 6. Intensity as a function of Re, for f = .003 and RNG.

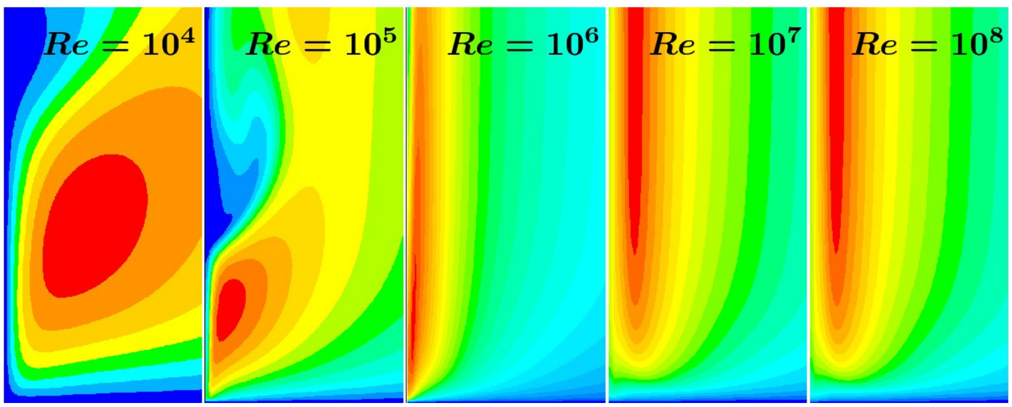

Figure 7. From the solutions in figure 6, *v* as a function of Re, for *f*=.003 and RNG. Contour interval is 0.1. Region shown is *z*=.105 to *r*=.055.

For laminar vortices, Fiedler [2] shows that the value of f that maximizes intensity is approximately $f = Re^{-1/3}$, which gives f = .002 for $Re = 10^8$. Figure 5 shows intensity is maximized for RSM and RNG near f = .003. Surely this close agreement with the laminar formula must be somewhat fortuitous, given that the solutions here, and hence the optimal value of f , become independent of Re for $Re > 10^7$. Likewise, our results indicate that the similarity theory of Nolan [14], which still retains dependence on viscosity (and hence Re) would need to be modified for applications to tornadoes.

Figure 8 shows the turbulent intensity ($\sqrt{2k}/U$, where U is the resolved speed) and the turbulent viscosity μ_t in simulations with the four turbulence models. Note the $k-\varepsilon$ model predicts substantially larger values of both these quantities at the base of the updraft, consistent with the production of only a wide, weak vortex with $k-\varepsilon$. Yet at the top of updraft, $k-\varepsilon$ performs similarly to RSM. The three schemes that produce strong vortices have reduced turbulent viscosity both in and around the vortex. Only the RNG scheme suppresses turbulent viscosity where the updraft impinges on the upper boundary.

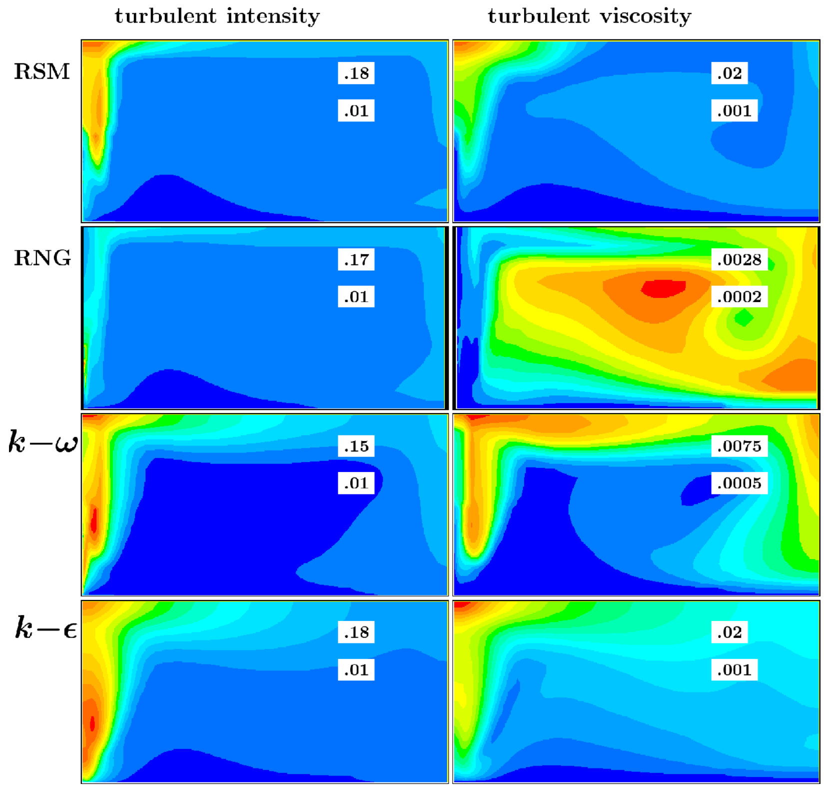

Figure 8. Turbulent intensity and turbulent viscosity for selected simulations with *f*=.003 and Re=10^8, essentially the simulations in the third column of figure 5. The entire domain is shown.

3.1. Additional Turbulence Models

Figure 9 shows intensity for Re = 10^8 and f =.003, for the four turbulence models discussed above ($k{-}\varepsilon$, $k{-}\omega$, RNG and RSM) but also five modifications of those models. Jiao et al. [15] suggest modifications of the coefficients for RSM, based on attempts with **FLUENT**$^{\text{TM}}$ to simulate measurements within an industrial cyclone, with a diameter of 0.15 m [16]. Based on the diameter of the cyclone (rather than the width of inlet), the Reynolds number ranged from Re = $6{\times}10^4$ to Re = 1.3 $\times 10^5$. They suggest some rather drastic modifications of the default RSM coefficients, which for their simulations improved the representation of the fluctuating flow field, while retaining the good performance of the standard RSM model with the time-mean flow field. In Figure 9, the simulation with the coefficients of Jiao et al. (2007) is labeled "mod RSM". Though we find a significant impact on the intensities, the structure of the vortex remains the same: a vortex with an axial jet sustaining a vortex breakdown aloft.

In Section 1.2, the hybrid RNG model of Saqr *et al.* [5] was cited. The simulation with that model is labeled "hybrid RNG", and produces very little difference from RNG, consistent with the statement of Saqr et al. [5] that the primary difference between RNG and $k{-}\varepsilon$ is the presence of R_ε in the RNG model, rather than the "derived" coefficients.

Within RNG, **FLUENT**$^{\text{TM}}$ offers an option for "swirl dominated flow", the details of which are not available to the user. That option was used for all RNG simulations, except for the one here marked "nsm RNG" (nsm being an abbreviation for "no swirl modification"). We thus conclude that the option for "swirl dominated flow" has no significant effect on these simulations. Likewise, **FLUENT**$^{\text{TM}}$ offers an adjustable swirl factor α_s, the default value of which is $\alpha_s = 0.07$. We find (not plotted) that I_v is reduced by 6% with $\alpha_s = 0.11$ and increased by 31% when $\alpha_s = 0$.

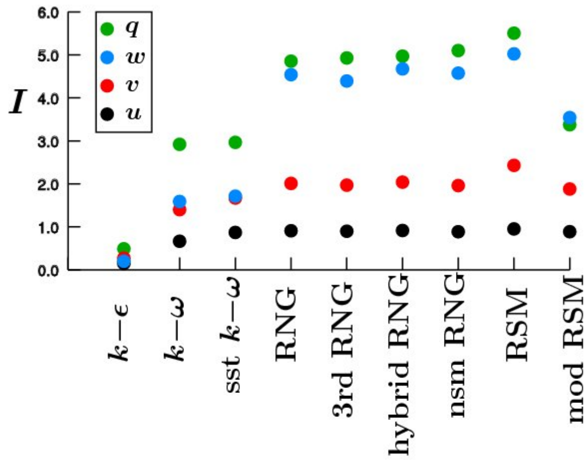

Figure 9. Intensity as a function of turbulence model with *f*=.003, with variations on the standard four turbulence models.

For no particular reason, except as a legacy from our first simulations, all simulations here used first order advection for k and ε, except for "3rd RNG", in which the 3rd order MUSCL advection scheme was used for k and ε, with no significant effect. We also mention (but do not plot) that if the QUICK advection scheme is employed in RNG, for all advection, I_v is reduced 17%.

Lastly, we include $k-\omega$ with the shear-stress transport option available within **FLUENT™**, in the simulation marked "sst $k-\omega$". From the description of the option within the User's Guide, there is no particular reason to recommend it for a vortex. We find no significant impact, as compared with $k-\omega$.

4. Conclusions

A commercial CFD code, **FLUENT™**, has been applied to a vortex within an updraft above a frictional lower boundary. **FLUENT™** has been widely used by others in simulations of engineering turbulent flows and verified against experiments, though the experiments cited in this regard generally have a Reynolds number of $Re = 10^5$ or less. Most of the simulations here employed a Reynolds number of the updraft of $Re = 10^8$. In a series of laboratory simulations of tornadoes in the 1970s and 1980s, the typical Reynolds number was $Re \approx 2\times10^4$ [17]. So the simulations here are outside the bounds of easy laboratory confirmation, and instead approach the Reynolds number of real tornadoes.

The simulations here employed the variety of turbulence models available within **FLUENT™**. The simulations were constrained to be axisymmetric. The vortex within the updraft has features similar to those that have been well-studied in axisymmetric simulations of laminar vortices. A noteworthy feature is that, within a certain range of input of swirl, the friction-induced convergence produces an axial jet in the core of the vortex, with the jet terminating at a vortex breakdown aloft. Fiedler and Rotunno [10] explain the essential role of the vortex breakdown in maintaining the low pressure in the core of the vortex beneath the breakdown point. Remarkably, the vortices here can be more intense than in previously studied laminar solutions. For example, in Fiedler [2] $I_q < 2.7$ in the axisymmetric solutions at $Re=4\times10^4$ while here $I_q > 4.5$ for several turbulence models, as seen in Figure 9. The more detailed (and computationally expensive) the turbulence model, the stronger the vortex, with RSM narrowly edging out RNG. Those two models suppress turbulent diffusion and stress within the strong vortex, relative to what occurs outside the vortex. Lewellen *et al.* [12] saw a need to include some rotational damping effects in an LES subgrid model to achieve favorable results. This research indicates, by its results, that the modern RSM and RNG models apparently include a mechanism for rotational damping, and there is no evidence that they need further modification to produce more rotational damping.

Using the updraft wind speed scale of 50 m s^{-1} for strong thunderstorm, a value of I_v=2 (as found with RNG and RSM) implies an azimuthal wind speed in a tornado of 100 m s^{-1}, consistent with the scales cited in Bluestein [1]. Is rotational damping of turbulence a key to the destructive intensity of real tornadoes, as it is for these axisymmetric simulations? The answer to that question is related to an additional question as to whether the destructive intensity of these simulations holds up in more expensive three-dimensional simulations. That latter question is provisionally answered with reference to the laminar simulations in Fiedler [2], in which the time-average intensity in three-dimensional solutions was slightly greater than that in the axisymmetric counterpart, and the largest intensities occurring over a broader range of f, with the range of f extending into lower values.

Acknowledgments

This work was supported by National Science Foundation (USA) Grant ATM-0646914. Several anonymous reviewers made significant contributions in an earlier submission.

Nomenclature

α_s	swirl factor
C_μ	model coefficient
ε	rate of dissipation of turbulent kinetic energy
f	2Ω, Coriolis parameter
I_q	maximum of q
I_u	maximum of u
I_v	maximum of v
I_w	maximum of w
k	tubulent kinetic energy
μ_t	eddy viscosity
ρ	mass density
p	pressure deviation
r	radial coordinate
z	vertical coordinate
u	radial velocity component
v	azimuthal velocity component
w	vertical velocity component
Re	Reynolds number
R_ε	additional rate of dissipation of ε term in RNG model
U	resolved speed
ω	specific dissipation rate
Ω	rotation rate of the coordinate system

References

[1] Bluestein, H. B., *Advances in applications of the physics of fluids to severe weather systems*. Rep. Prog. Phys., 2007. **70**, p. 1259-1323.

[2] Fiedler, B. H., *Suction vortices and spiral breakdown in numerical simulations of tornado-*

like vortices. Atmos. Sci. Let., 2009. **10(2)**, p.109–114.
[3] Bartosiewicz, Y., Z. Aidoun, P. Desevaux, and Y. Mercadier, *Numerical and experimental investigations on supersonic ejectors*. Int. J. Heat Fluid Flow, 2005. **26(1)**, p. 56 – 70.
[4] Gupta, A. and R. Kumar, *Three-dimensional turbulent swirling flow in a cylinder: Experiments and computations*. Int. J. Heat Fluid Flow, 2007. **28(2)**, p. 249–261.
[5] Saqr, K.M., Aly, H.S., Wahid, M.A., and Sies, M.M., *Numerical simulation of confined vortex flow using a modified k-epsilon turbulence model*. CFD Letters, 2009. **1(2)**, p. 87–94.
[6] Xiang, R. and K. Lee, *Numerical study of flow field in cyclones of different height.* Chem. Eng. and Process., 2005. **44(8)**, p. 877 – 883.
[7] Hoekstra, A. J., J. J. Derksen, and H. E. A. Van Den Akker, *An experimental and numerical study of turbulent swirling flow in gas cyclones*. Chem. Eng. Sci., 1999. **54**, p. 2055–2065.
[8] Fiedler, B. H., *The thermodynamic speed limit and its violation in axisymmetric numerical simulations of tornado-like vortices*. Atmos. Ocean, 1994. **32**, p. 335–359.
[9] Fiedler, B. H., *Wind-speed limits in numerically simulated tornadoes with suction vortices*. Q. J. Roy. Meteorolog. Soc., 1998. **124(551)**, p. 2377–2392.
[10] Fiedler, B. H. and R. Rotunno, *A theory for the maximum windspeeds in tornado-like vortices*. J. Atmos. Sci., 1986. **43(21)**, p. 2328–2340.
[11] Lewellen, D. C. and W. S. Lewellen, *Near-surface intensification of tornado vortices*. J. Atmos. Sci., 2007. **64(7)**, p. 2176–2194.
[12] Lewellen, D.C., W. S. Lewellen, and J. Xia, *The influence of a local swirl ratio on tornado intensification near the surface.* J. Atmos. Sci., 2000. **57(4)**, p. 527–544.
[13] Wyngaard, J. C., *Turbulence in the Atmosphere,* Cambridge University Press, 2010 p. 49
[14] Nolan, D. S., *A new scaling for tornado-like vortices.* J. Atmos. Sci., 2005. **62(7)**, p. 2639–2645.
[15] Jiao, J., Z. Liu, and Y. Zheng, 2007: *Evaluations and modifications on reynolds stress model in cyclone simulations*. Chem. Eng. Technol., **30(1)**, p. 15–20.
[16] Liu, Z., Y. Zheng, L. Jia, J. Jiao, and Q. Zhang, *Stereoscopic PIV studies on the swirling flow structure in a gas cyclone.* Chem. Eng. Sci., 2006. **61(13)**, p. 4252 – 4261.
[17] Pauley, R. L., *Laboratory measurements of axial pressures in two-celled tornado-like vortices.* J. Atmos. Sci., 1989. **46(21)**, p. 3392–3399.